Effect of Different Temperatures and Pore Pressures on Geomechanical Properties of Pore-Filling Type of Methane Hydrate Soils Based on the DEM Simulations

J. He, M.J. Jiang and J. Liu

Abstract Research is being conducted on the geomechanical properties of methane hydrate bearing soil due to increasing global energy demands. Mechanical behaviors of MHBS are greatly influenced by the temperature and pore pressure and it can only exist under a condition of low temperature and high pressure. It is of great significance to investigate such influences for the safe exploration of methane hydrate. This paper presents a numerical approach to study the mechanical properties of pore-filling type of MHBS under the influences of temperature and pore pressure by conducting DEM drained triaxial compression tests. The results show as the temperature decreases or pore pressure increases, the strength and elastic modulus of MHBS gradually increase, and the volumetric response switches from contractive to dilative. The direction of the contact between the particles forwards a vertical deflection with the development of the axial strain. The evolution rule of deviator fabrics of the strong contact $F^s_{11} - F^s_{33}$ is similar to that of stress ratio q/p-axial strain. The macro behavior changes along with the micro response.

1 Introduction

Methane hydrate bearing soil (MHBS), a specific natural soil deposit containing methane hydrate (MH) in its pores, is referred as one of the potential sources of green energy for solving the current global energy crisis. MHBS occurs in abun-

J. He (✉) · M.J. Jiang · J. Liu
State Key Laboratory for Disaster Reduction in Civil Engineering, Tongji University, Shanghai 200092, China
e-mail: 12hejie@tongji.edu.cn

J. He · M.J. Jiang · J. Liu
Key Laboratory of Geotechnical and Underground Engineering of Ministry of Education, Tongji University, Shanghai 200092, China

J. He · M.J. Jiang · J. Liu
Department of Geotechnical Engineering, Tongji University, Shanghai 200092, China

© Springer Science+Business Media Singapore 2017

X. Li et al. (eds.), *Proceedings of the 7th International Conference on Discrete Element Methods*, Springer Proceedings in Physics 188,
DOI 10.1007/978-981-10-1926-5_86

dance under permafrost regions and deep seabed [1]. MH can be formed in soil pores under high pressure and low temperature.

In the commercial exploration of MH, the strength of MHBS may deteriorate after changing temperature–pressure conditions using thermal stimulation, depressurization, or inhibitor injection [2]. This can trigger a series of geotechnical engineering disasters, like the collapse mining platforms and auxiliary facilities, even potentially inducing submarine landslide or tsunami [3]. Therefore, it is of great importance to investigate the influence of temperature and pore pressure on the mechanical properties of MHBS to successfully achieve exploitation of MH.

Previous studies show that the mechanical properties of MHBS depend highly on different hydrate morphology (e.g., pore-filling, load bearing and cementation) [1, 4, 5]. Marine sandy sediments containing pore-filling MH particles can be considered as a class of special granular materials that present apparent obvious discontinuity characteristics. The distinct element method (DEM) [6] can be used by modeling MH particles as agglomerates of spheres cemented together and filled into the pores of soil skeleton based on the specific MH saturation. In this study, a pore-filling type of MHBS with specific MH saturation is generated by using a novel technique. Then, the drained triaxial compression tests with different pore pressures and temperatures are conducted to analyze its stress-strain and volumetric responses and contact fabric.

2 Numerical Simulation

MH saturation is defined by the ratio of MH volume to the total pore volume. Namely:

$$S_{mh} = \frac{V_{mh}}{V_v} \times 100\,\% \tag{1}$$

where V_{mh} is the volume occupied by MH; and V_v is the total pore volume.

A new technique for generating the pore-filling type of MHBS has been proposed by He and Jiang [7]. We briefly introduce this method in this paper to simplify the reader's understanding.

As illustrated in Fig. 1a, a homogeneous DEM cubic sample with an initial void ratio of 0.84 was generated by using the multi-layer under-compaction technique [8]. The size of the cubic specimen is $5.445 \times 5.445 \times 5.445\,\text{mm}^3$. The particle size distribution of soil used in the DEM simulations, as shown in Fig. 1b, is close to Toyoura sand particle size in order to better simulate the real situation. The range of particle diameter is 0.1–0.42 mm, and the number of soil particle is set to be 10,000.

MH particles are generated within the scope of a sphere with radius of R_a, and then cemented together as a whole, forming a cluster of MH. Meanwhile, the void ratio e_a in the sphere can be calculated as follows:

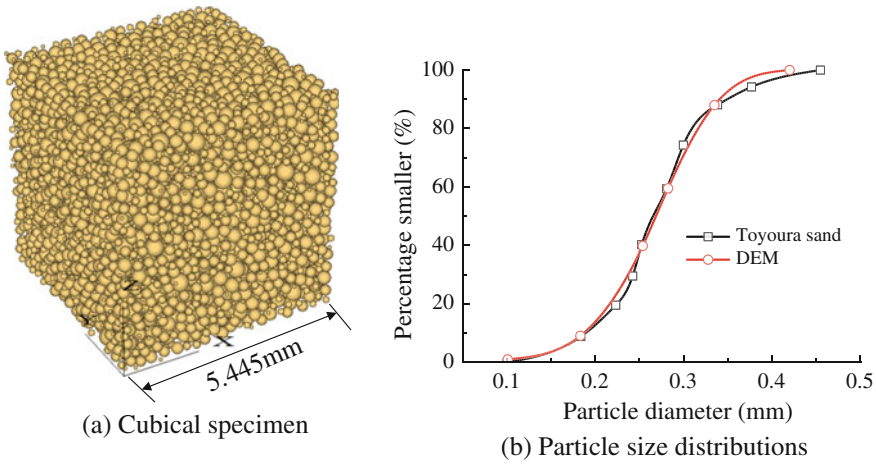

(a) Cubical specimen

(b) Particle size distributions

Fig. 1 A cubical specimen in the DEM simulations with particle size distributions close to Toyoura sand in laboratory tests

$$e_a = \frac{\frac{4}{3}\pi R_a^3 - \frac{4}{3}\pi r^3 \times n}{\frac{4}{3}\pi r^3 \times n} \tag{2}$$

where r is the radius of MH particle; n is the number of MH in the sphere.

Then, R_a can be obtained by (3):

$$R_a = \left[(1 + e_a) \times r^3 \times n\right]^{\left(\frac{1}{3}\right)} \tag{3}$$

In the MHBS specimen, the following equations are satisfied:

$$\begin{aligned} V_{mh} &= N \times V_a \\ V_a &= \frac{4}{3}\pi r^3 \times n \times (1 + e_a) \end{aligned} \tag{4a, b}$$

where V_a is the volume of a single MH cluster; N is the number of MH clusters in the pore of soil sample.

Based on (4a, b), the number of MH clusters N can be calculated by (5).

$$N = \frac{V_{mh}}{\frac{4}{3}\pi r^3 \times n \times (1 + e_a)} \tag{5}$$

The void ratio e_a, radius r of MH particle and the number of MH particles n are set to be 0.82, 0.024 and 60 mm, respectively. Firstly, N spherical particles are randomly generated in the pore of soil sample, subsequently, 60 small MH particles with the radius of 0.024 mm are generated in the scope of a sphere, and then

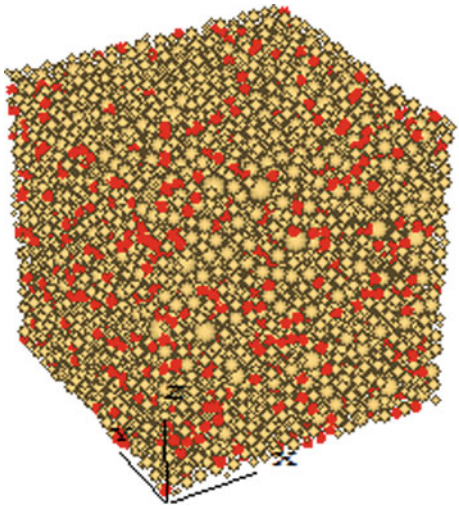

Fig. 2 3D DEM specimen of pore-filling type of MHBS with $S_{mh} = 15\,\%$

cemented together to form a cluster of MH, as illustrated in Fig. 2. The parallel bond model (PBM) is used in this paper. For $S_{mh} = 15\,\%$ of MHBS, the number of MH clusters N is 1728. Table 1 lists the adopted material parameters used in our simulations.

3 Numerical Results

The mechanical behavior of MHBS is greatly influenced by the existing environment, i.e., temperatures and pore pressures. In [9], the cementation parameters of PBM are determined under the condition of a given temperature and pressure state. The different values of cementation parameters of PBM can be chosen to represent different temperatures and pore pressures of MHBS. A serial of drained triaxial compression tests was then conducted to simulate the mechanical response of MHBS under different temperatures and pore pressures.

3.1 Effect of Pore Pressure

Figure 3 shows the influence of different pore pressures (i.e., 2, 3 and 6 MPa) on the deviator stress, axial strain, and volumetric strain relations for MHBS with $S_{mh} = 15\,\%$ under condition of effective confining pressure of 1.5 MPa and temperature of $-30°$. As illustrated in Fig. 3a, the deviator stress and elastic modulus of MHBS gradually increase with the increases of Pore pressure. The deviator stress increases to a peak value and exhibits a slight post-peak strain softening. As axial

Table 1 Parameters of granules in the DEM

Parameters	Value	Parameters	Value
Soil density/(g/cm^3)	2.65	Wall normal stiffness/(N/m)	1.5×10^5
MH density/(g/cm^3)	0.9	Wall tangential stiffness/(N/m)	1.0×10^5
Soil normal contact stiffness k_n^p/(N/m)	1.5×10^5	MH normal contact stiffness k_n^p/(N/m)	1.5×10^4
Soil tangential contact stiffness k_s^p/(N/m)	1.0×10^5	MH tangential contact stiffness k_s^p/(N/m)	1.0×10^4
Soil inter-particle coefficient of friction μ^p	0.5	MH inter-particle coefficient of friction μ^p	0.04

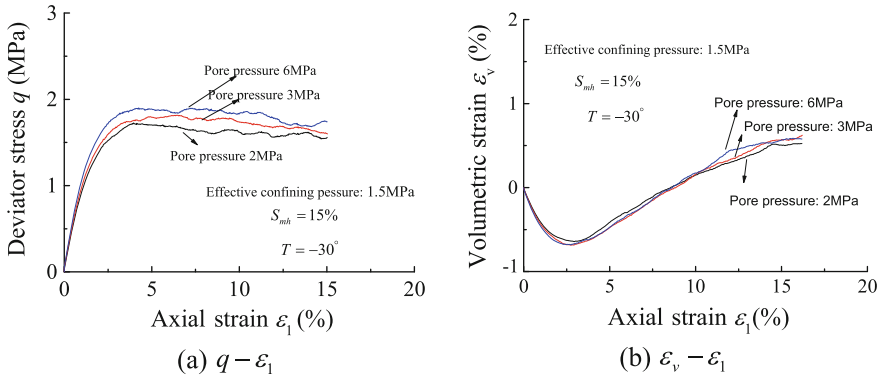

Fig. 3 Effect of pore pressure on the deviator stress-volumetric strain-axial strain relation for pore-filling type of MHBS with $S_{mh} = 15\,\%$

strain increases, the MHBS experiences a transition from volumetric compression to volumetric dilatancy, as shown in Fig. 3b.

3.2 *Effect of Temperatures*

Figure 4 shows the effect of temperatures (i.e., $T = -10°, -20°, -30°$) on the deviator stress, axial strain, and volumetric strain relations for MHBS with $S_{mh} = 15\,\%$ at the effective confining pressure of 1.5 MPa and pore pressure of 3 MPa. In Fig. 4a, the deviator stress reaches a peak value and exhibits a slight post-peak strain softening. The deviator stress of MHBS gradually decreases with temperatures increase. All the specimens experience an overall dilation during shear, as shown in Fig. 4b.

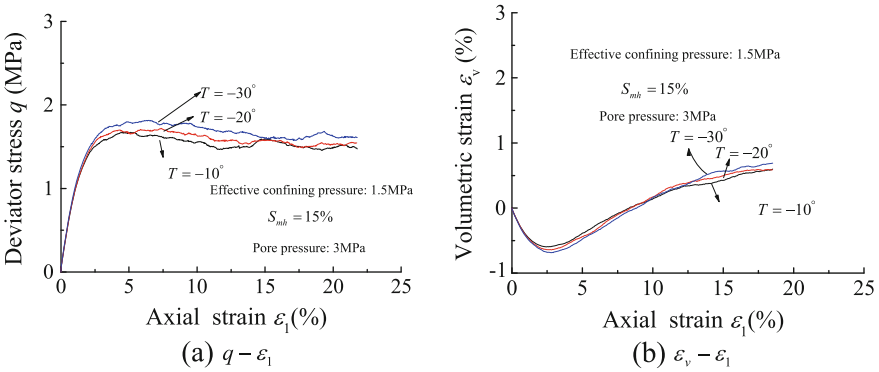

Fig. 4 Effect of temperatures on the deviator stress, axial strain and volumetric strain relations for pore-filling type of MHBS with $S_{mh} = 15\,\%$

3.3 Macro-Micro Relationship

The unit normal vector for all contacts is defined based on Satake [10]:

$$F_{ij} = \frac{1}{N_c}\sum_{k=1}^{N_c} n_i^k n_i^k, i = j = 1, d \tag{6}$$

where N_c is the number of contacts; n_i^k is the component of the unit vector n^k at a contact; and d is equal to 3 for 3D.

The unit normal vector for the strong contacts is described by Kuhn [11]:

$$F_{ij}^s = \frac{1}{N_c}\sum_{s=1}^{N_c^s} n_i^s n_j^s, i = j = 1, d \tag{7}$$

where N_c^s is the number of the strong contacts; and n_i^s is the component of the unit vector n^s at a strong contact. It refers to as a strong contact if the normal contact is greater than the average normal contact force f_{ave}^n. The average normal contact force is calculated by the following equation.

$$f_{ave}^n = \frac{1}{N_c}\sum_{i=1}^{N_c} f_i^n \tag{8}$$

where f_i^n is the normal contact force.

Figure 5 presents the evolution of the strong contact (i.e., F_{11}^s, F_{22}^s, and F_{33}^s) for pore-filling type of MHBS with $S_{mh} = 15\,\%$ under pore pressure of 3 MPa and effective confining pressure of 1.5 MPa at $T = -30^\circ$. With axial strain increases, F_{11}^s reaches a peak value and then decreases to a steady value, while F_{22}^s and F_{33}^s

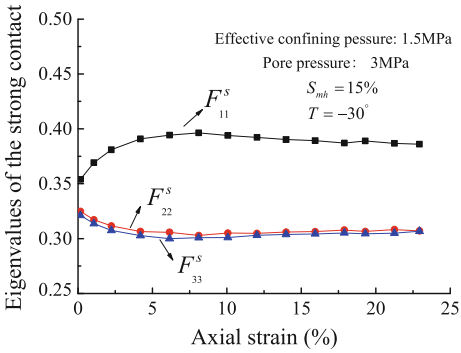

Fig. 5 Evolution of eigenvalues of the strong contact for pore-filling type $S_{mh} = 15\,\%$

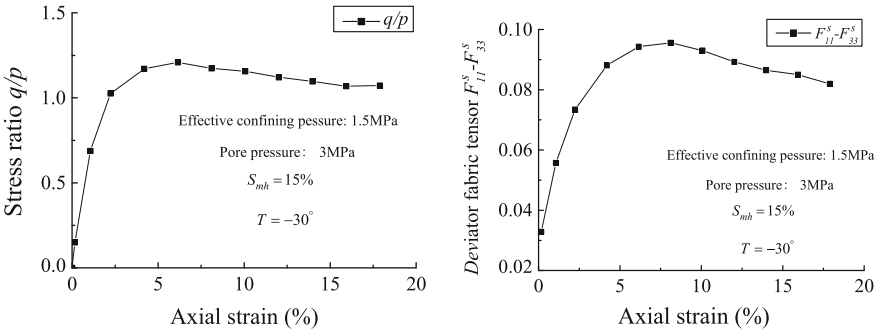

(a) stress ratio q/p (b) deviator fabric tensor $F^s_{11} - F^s_{33}$

Fig. 6 Relations between stress ratio q/p, deviator fabric tensor $F^s_{11} - F^s_{33}$ and axial strain for pore-filling type $S_{mh} = 15\,\%$

gradually decrease to a minimum, then slight increase to a constant. The evolution of F^s_{11} represents the direction of the contact between the particles forwards a vertical deflection with the development of the axial strain.

Figure 6 shows relations between the stress ratio q/p, deviator fabrics of the strong contact $F^s_{11} - F^s_{33}$, and axial strain under the same condition (i.e., $S_{mh} = 15\,\%, T = -30^\circ$, pore pressure of 3 MPa, and effective confining pressure of 1.5 MPa). As shown in Fig. 6, the evolution rule of deviator fabrics of the strong contact $F^s_{11} - F^s_{33}$ is similar to that of stress ratio q/p-axial strain. The macro behavior changes along with the micro response.

4 Conclusions

The DEM simulation can effectively capture the macro-mechanical response of stress–strain and volumetric strain of MHBS in different temperature and pore-pressure conditions. As the temperature decreases or pore pressure increases, the strength and elastic modulus of MHBS gradually increase, and the volumetric response switched from contractive to dilative. F_{11}^s reaches a peak value and then decreases to a steady value, while F_{22}^s and F_{33}^s firstly decrease to a minimum, then slight increase to a stable value. The direction of the contact between the particles forwards a vertical deflection with the development of the axial strain. The macro behavior changes along with the micro response. The evolution rule of deviator fabrics of the strong contact $F_{11}^s - F_{33}^s$ is similar to that of stress ratio q/p-axial strain.

Acknowledgments The research was funded by the National Natural Science Foundation of China with grant Nos. 51179128, 51579178, Project of State Key Laboratory for Disaster Reduction in Civil Engineering, Tongji University, of China with grant No. SLDRCE14-A-04. All the supports are greatly appreciated.

References

1. Soga, K., Lee, S.L., Ng, M.Y.A., Klar, A.: Characterisation and engineering properties of methane hydrate soils. In: Characterisation and Engineering Properties of Natural Soils, vol. 4, pp. 2591–1642. Taylor and Francis, London (2006)
2. Demirbas, A.: Methane hydrates as potential energy resource: Part 2—Methane production process from gas hydrates. Energ. Convers. Manage. **51**, 1562–1571 (2010)
3. Sultan, N., Cochonat, P., Foucher, J.P., Mienert, J.: Effect of gas hydrates melting on seafloor slope instability. Mar. Geol. **213**, 379–401 (2004)
4. Brugada, J., Cheng, Y., Soga, K., Santamarina, J.: Discrete element modelling of geomechanical behaviour of methane hydrate soils with pore-filling hydrate distribution. Granul. Matter **12**, 517–525 (2010)
5. Jiang, M.J., He, J., Wang, J.F., Chareyre, B. Zhu, F.Y.: DEM analysis of geomechanical properties of cemented methane hydrate bearing soils at different temperatures and pore pressures. Int. J. Geomech. (ASCE) (2015). (SCI Source J.). http://ascelibrary.org/doi/abs/10.1061/(ASCE)GM.1943-5622.0000612
6. Cundall, P.A., Strack, O.: A discrete numerical model for granular assemblies. Géotechnique **29**, 47–65 (1979)
7. He, J., Jiang, M.J.: Three-dimensional distinct element novel sample-preparing method and mechanical behavior of pore-filling type of methane hydrate-bearing soil (2016, accept for publication)
8. Jiang, M.J., Konrad, J.M., Leroueil, S.: An efficient technique for generating homogeneous specimens for DEM studies. Comput. Geotech. **30**, 579–597 (2003)
9. Jiang, M., He, J.: Three-dimensional distinct element simulation of macro triaxial compressional strength characteristics of methane hydrate through uniaxial compressional test. Rock Soil Mech. **35**(9), 2692–2701 (2014). (In Chinese)

10. Satake, M.: Fabric tensor in granular materials. In: Vermeer, P.A., Luger, H.J. (eds.) Proceedings of IUTAM Symposium on Deformation and Failure of Granular materials, Balkema, Delft, The Netherlands, pp. 63–68 (1982)
11. Kuhn, M.R.: OVAL and OVALPLOT: programs for analyzing dense particle assemblies with the discrete element method (2006)